JOURNAL OF APPLIED ELECTROCHEMISTRY **26** (1996) 575–583

Oxidation of arsenopyrite (FeAsS) in acid Part I: Reactivity of arsenopyrite

P. G. FERNANDEZ

School of Applied Chemistry, Curtin University, Bentley, Australia 6102

H. G. LINGE*

CSIRO DMP, Curtin University, Bentley, Australia 6102

M. W. WADSLEY

Dept. of Chemical Engineering, Monash University, Clayton, Australia, 3168

Received 19 June 1995; revised 24 November 1995

The oxidation reactivity of arsenopyrite FeAsS in dilute acid determines the recovery of gold from arsenopyritic gold ores by slurry electrolysis. Stoichiometric,sulfur- and arsenic- deficient arsenopyrite have practically the same oxidation rate. Arsenopyrite is covered with a metal deficient sulfide layer which appears to determine the restpotential of the electrode. This layer can be separately oxidized and reduced during bulk-oxidation of arsenopyrite. Arsenopyrite oxidation is accelerated by dissolved Na_2SO_4 and by high electrode potentials and solution acidity. The rate is controlled by a surface reaction with an apparent activation energy of 33 kJ mol^{-1}.

1. Introduction

Arsenopyrite is an iron–arsenic–sulfide (FeAsS) frequently containing gold which cannot be extracted by cyanidation unless the arsenopyrite matrix is decomposed [1]. This study investigated the electrochemical oxidation of arsenopyrite as a means to decompose arsenopyrite electrolytically in dilute acid [2] and is reported in two parts. The first paper explores conditions for which arsenopyrite has a high oxidation reactivity. The second paper [3] explores the reaction stoichiometry and likely reaction scheme for acidic chloride solutions, which is the most likely practical medium for the electrolytic processing of arsenopyritic gold ore [1,2,4].

There are many reviews of the electrochemical decomposition of metal sulfides (e.g., [5–7]). Electrochemical oxidation of arsenopyrite has been studied previously [8–16]. Kostina and Chernyak [8–10] concluded that the reaction was more pronounced in alkali than in acid. Sisenov *et al.* [12] suggested that arsenopyrite is covered by a passive layer of elemental sulfur in acid and by an iron hydroxide layer in neutral and alkaline solution. There is a broad concensus [11,13–16] that in alkali (pH $\geqslant$ 11) arsenopyrite oxidizes as in Reaction 1:

$$FeAsS + 11H_2O \longrightarrow Fe(OH)_3 + HAsO_4^{2-} + SO_4^{2-} + 18H^+ + 14e^- \quad (1)$$

* Author for correspondence at PO Box 482, Kalamunda, Australia, 6076

but there has been little work published on the oxidation of arsenopyrite in acid. Kostina and Chernyak [8] indicated that arsenopyrite oxidation in sulfuric and hydrochloric acid was insignificant until the potential exceeded 1 V vs SHE. Jackson and Strickland [17] studied the oxidation of an arsenopyrite slurry using acidic chlorine water at pH 1 and stated that temperature had little effect on the oxidation rate, but no data were given. Papangelakis and Demopoulos [18] studied the mechanism of pressure oxidation of arsenopyrite in oxygenated 0.25 M sulfuric acid between 120–180 °C. The activation energy was 64 kJ mol^{-1}, assigned to a rate controlling oxygen reduction step on the arsenopyrite surface (the 'cathodic part reaction'). This study therefore gives no information on the intrinsic rate of arsenopyrite oxidation (the 'anodic part reaction') as this step was evidently too fast. Thus, although there have been studies of arsenopyrite oxidation in acid and alkaline solutions, many of its electrochemical properties remain uncertain.

This work examines the effect of pH, background electrolyte composition, temperature, mineral stoichiometry [19] and reaction time on the oxidation of arsenopyrite in acidic solution. Our measurements [20] of the oxidation of arsenopyrite in alkali confirm that there is insignificant reaction between pH 6–10 [13–16] and indicate that the rate of reaction (1) at pH 11–13 is controlled by the diffusion of OH^- to the arsenopyrite surface.

2. Experimental details

AR grade chemicals (purity by label >99%) and

0021-891X

Milli-Q (Millipore) water were used to make up background electrolytes. Solutions were adjusted to a desired pH with dilute hydrochloric acid. pH was measured with a commercial combination glass electrode and meter (Metrohm).

Arsenopyrite minerals can be sulfur- or arsenic-deficient [20,21]. Natural samples from Greenbushes (Australia), Wuhan (China) and Santa Eulalia (Mexico) covered this range and were used to test the influence [19] of mineral stoichiometry on the rate of oxidation. Sample composition was measured by X-ray diffraction (XRD), dispersive X-ray analysis (SEM/EDX) and wet chemical analysis [20]. The composition was as follows: Greenbushes $Fe_{1.00}As_{1.00}S_{1.00}$, Wuhan $Fe_{1.00}As_{1.00}S_{0.94}$ and Santa Eulalia $Fe_{1.00}As_{0.92}S_{1.00}$. For all samples, a thin gold layer was sputtered on one surface and a copper wire cemented to this surface with silver epoxy resin (Epoxy Technology). The copper wire was enclosed in a glass tube which rested on the electrode surface contact and the lower section was encapsulated in epoxy resin (Epirez Australia). The arsenopyrite surface opposite the electrical contact was ground flat on wet silicon carbide paper using, progressively, grade 240 (coarse)–600 (fine) before a final polish on wet Buehler Microcloth (Buehler).The geometric surface area of the electrode was calculated from the dimensions of the exposed surface measured under low magnification (×10) and were: $\sim 0.02\,cm^2$ for Greenbushes samples; ~ 0.2–$0.5\,cm^2$ for Wuhan and Santa Eulalia samples. Electrode resistances were $\sim 50\,\Omega$ (Greenbushes samples) and $\sim 2\,\Omega$ (Wuhan and Santa Eulalia samples), yielding specific resistances in the range 2–$5\,\Omega\,cm^{-1}$.

The current–potential response was measured potentiostatically in a thermostated glass cell ($\sim 100\,cm^3$ capacity) using conventional equipment (Pine type RDE 3 potentiostat-sweep generator, Hewlett Packard X–Y and Yew X–t recorders) and a three electrode system consisting of the arsenopyrite working electrode, a platinum counter electrode (electrode area $\sim 2\,cm^2$) and an SCE reference electrode (Metrohm type 60701.000, positioned outside the cell). When logarithmic current display was required, the current–voltage converter on the potentiostat was adjusted manually at appropriate points and the data read from the X–Y trace. Current density was displayed semilogarithmically using a computer and iR corrections subtracted from the applied potential using the resistance of the electrode. Potentials in this paper are expressed relative to SHE using the value 0.244 V for SCE vs SHE [22].

The cell was purged of dissolved oxygen with ultrapure nitrogen (CIG, Australia). Cell solutions were stirred magnetically at 300 rpm unless otherwise stated. In some experiments, the oxidized electrode was periodically removed, dried and examined with a microscope. Product layers on the electrode were scraped off and characterized using SEM/EDX and XRD.

3. Results and discussion

3.1. *Exploratory voltammetry*

Figure 1 gives typical oxidation current density–potential curves, shown for Santa Eulalia samples for various experimental conditions. Each curve was obtained with a freshly ground electrode surface allowed to reach a steady restpotential (referred to as 'conditioned' electrode), which was always more positive than the potential measured when the electrode was first immersed in the solution (e.g., within about 1 min of electrode surface preparation, referred to as 'fresh' electrode). Figure 1(a) shows that anodic current could be passed at a lower potential for a fresh electrode than for a conditioned electrode, although the curves eventually converged at higher potentials. For all conditions, solution stirring had no influence on the current. Increasing temperature enhanced the current. Figure 1(b) illustrates the influence of different electrolytes at pH 2, 25 °C. Addition of Na_2SO_4 to $NaClO_4$ and NaCl (not shown), simulating the influence from SO_4^{2-} produced in the oxidation of arsenopyrite [3], increased the current. Similarly, increasing [NaCl] between 0.01 and 1 M, simulating salinity differences in prospective plant liquors [4], also increased the current. Figure 1(c) shows the effect of pH for both 1 M $NaClO_4$ and 1 M NaCl solution at 25 °C. Increased acidity enhanced the current for both electrolytes at high potentials but the effect is apparently reversed at low potentials.

Figure 2 shows examples of forward and reverse sweeps, indicating significant hysteresis, especially for 1 M electrolyte. At high potentials, the current for the reverse sweep is greater than for the forward sweep, indicative of an increase in the real surface area of the electrode as a result of oxidation. Electrode conditioning has only a slight influence on this pattern, confined to a small additional anodic charge which can be passed at low potentials. On the reverse sweep the current declines rapidly to cross the current axis positive to the original restpotential (e.g., 0.2 V more positive for 1 M NaCl at pH 2, 25 °C). When the potential sweep was stopped in this region, the current increased with time as shown by the transition A → B in Fig. 2. The open circles show the quasi-steady state current when an electrode was polarized in 1 M NaCl from the restpotential by a potential step to ~ 1 V (at higher potentials the current is largely controlled by the resistance of the electrode), with subsequent potential adjustment downwards to the restpotential. These currents are practically constant for minutes. The values lie between the forward and the reverse sweep and have been used to analyse the influence of experimental variables (see further below).

3.2. *Electrode restpotential and surface condition*

Figure 3 illustrates the potential-time dependence of arsenopyrite electrodes. For a fresh surface (A), the potential is steady within 10 min (shown for 1 h but

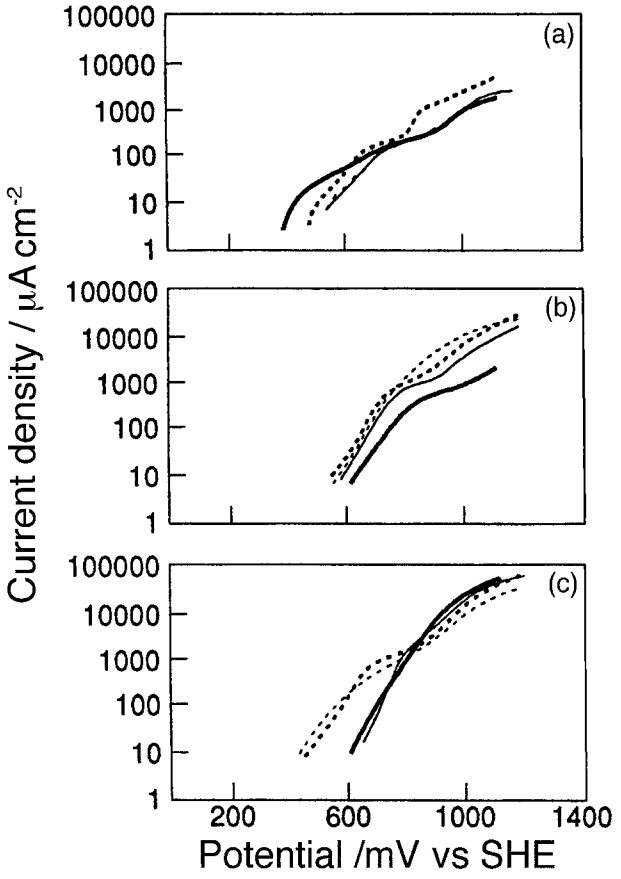

Fig. 1. Voltammogram for Santa Eulalia arsenopyrite in acid at $10\,mV\,s^{-1}$ (all curves relate to a conditioned surface in stirred solution at 25 °C except when stated otherwise). (a) Effect of solution stirring, electrode conditioning and temperature in 1 M NaCl, pH 2. Key: (----) 25 °C; (——) fresh surface; (——) nonstirred; (----) 75 °C. (b) Effect of electrolyte composition at 25 °C, pH 2 (0.01 M NaCl, 1 M NaCl, 1 M $NaClO_4$ and influence of added 0.15 M Na_2SO_4). Key: (——) 0.01 M; (----) 1 M NaCl; (——) 1 M $NaClO_4$; (----) 1 M $NaClO_4$/0.15 M SO_4. (c) Effect of pH (0.5–4) in 1 M NaCl or 1 M $NaClO_4$ at 25 °C. Key: (——) pH 0.5 NaCl; (----) pH 3 NaCl; (——) pH 1 $NaClO_4$; (----) pH 4 $NaClO_4$.

found to be valid for several hours in other experiments) and reproducible (±10 mV). There was insignificant change of the restpotential when the solution was aerated or in quiescent solution. This potential is therefore not a mixed potential involving the solution. The electrode response is slower to pH change after equilibration (B) or oxidation for several minutes at 1 V (C,D) than for a fresh surface. These trends suggest that the process establishing the surface condition for a fresh surface in the solution is different to the processes which operate after the electrode has been conditioned or oxidized.

The restpotential of arsenopyrite cannot be interpreted using E_h-pH diagrams (e.g., [11–16]) which are all based on Barton's [23] estimate of $-109.7\,kJ\,mol^{-1}$ for the free energy of formation of arsenopyrite at 25 °C. Barton's calculation is based on estimates of the activity of arsenic and sulfur in arsenic–sulfur melts in contact with solid arsenopyrite and pyrrhotite in the temperature range 491–702 °C. Barker and Parks [24] have since shown that Barton's calculation for sulfur activities over pyrrhotite disagree with more precise measurements. Barton also assumed that an arsenic-sulfur melt would be in equilibrium with solid arsenic and realgar (As_2S_2) at the eutectic temperature. This assumption is not in agreement with the determination of the arsenic-sulfur phase diagram by Blachnik *et al.* [25]. Consequently, Barton's calculation for the free energy of formation of arsenopyrite is, at best, a first order estimate with an unknown uncertainty. Calculations of the equilibrium potential of arsenopyrite for various decomposition reactions [11–16] at 25 °C, based on Barton's value, return significantly lower values over the whole pH range than restpotentials measured experimentally.

Figure 4 summarizes the dependence of the restpotential on pH and electrolyte composition including previous measurements for water [11], 0.6 M Na_2SO_4 [15, 16] and 0.1 M KH_2PO_4 [12]. Increasing pH generally decreases the restpotential. The data for water, $NaClO_4$ and Na_2SO_4 are reasonably concordant. NaCl and KH_2PO_4 decreased the potential. This evidence suggests that OH^-, Cl^- and phosphate ion stabilize the oxidized form of the surface phase on arsenopyrite. Na_2SO_4 additions (0.15 M) to 1 M $NaClO_4$ or 1 M NaCl solution did not affect the restpotential, even though SO_4^{2-} is a reaction product [3]. There is also no discernible effect from dissolved

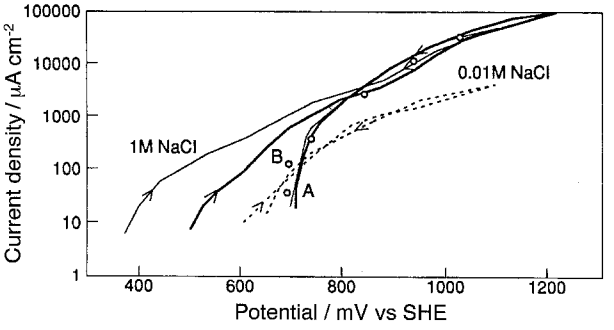

Fig. 2. Voltammogram of Santa Eulalia arsenopyrite in 0.01 or 1 M NaCl at pH 2, 25 °C. Hysteresis of forward and reverse sweep and effect of electrode preconditioning or quasi-steady state oxidation (open circles). For transition A ⟶ B see text. Key: (——) fresh surface, 1 M NaCl; (——) conditioned surface, 1 M NaCl; (– – –) conditioned surface, 0.01 M NaCl.

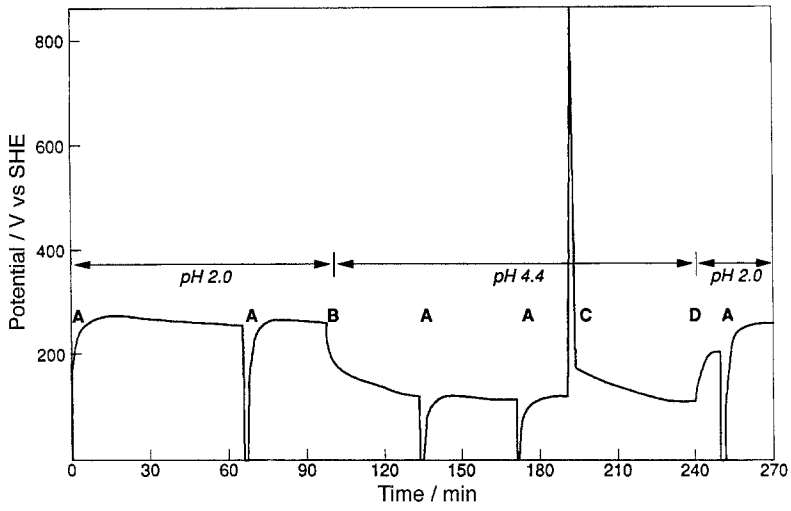

Fig. 3. Electrode potential-time dependence of Santa Eulalia arsenopyrite in 1 M $NaClO_4$/0.15 M Na_2SO_4 at pH 2–4.4 and 25 °C in stirred solution; A (fresh surface), B (conditioned surface), C and D (oxidation).

arsenopyrite. Addition of equimolar $FeCl_2/FeCl_3$ to yield concentrations $>10^{-3}$ M increased the arsenopyrite potential to match the value measured on Pt in the same solution; showing [26] that the dissolved redox couple Fe(II)/(III) determined the potential on the arsenopyrite surface for these conditions (tests for As(III)/As(V) addition were not made as this redox couple is irreversible [27]). Increased temperature decreased the restpotential in 1 M $NaClO_4$ at pH 2 by 35 mV (50 °C) and 100 mV (75 °C) indicating increased stability of the oxidized form of the surface phase at higher temperatures.

Analysis of the restpotential of arsenopyrite in neutral solution or alkali has been in terms of a surface layer which could not be reduced/oxidized at the restpotential [11–16] *unlike* the situation in acid. Figure 5 shows an example of cyclic reduction/oxidation of arsenopyrite at the restpotential (*P*) in acid. There are clear changes in the potential at zero-current between successive stages of reduction/oxidation from the restpotential, even for modest perturbations. In the first reduction cycle, 0.9 mC cm^{-2} was passed and the zero-current potential had decreased 12 mV from *P*. In the subsequent oxidation cycle, 0.3 mC cm^{-2} was passed and the zero-current potential had increased by 13 mV from *P*, even though there was net reduction of the electrode at this stage by 0.6 mC cm^{-2}. The zero-current potential, therefore, does not reflect a surface equilibrium. The same pattern holds for more extensive reduction/oxidation. In the second reduction cycle the charge passed was 8.6 mC cm^{-2}. The potential was held at A for 3 min and the decreasing reduction current in this interval AB was monitored. The zero-current potential on the continuing sweep had decreased by 87 mV from *P*. In the next oxidation cycle, 7.6 mC cm^{-2} was passed (again, the potential was held at C for 3 min and the decreasing oxidation current in this interval CD was monitored) and the potentiostat disconnected at D. The open-circuit potential jumped to *E*, which was 33 mV more positive than *P*, even though the electrode had been reduced by a net 1.6 mC cm^{-2} in the whole experiment. The open-circuit potential drifted slowly to lower values (similar to the pattern CD in Fig. 3) but this readjustment was not studied in detail. The decrease of the current at constant potential for both reduction/oxidation indicates that the reactions involved are self-limiting, as expected for a process confined to the electrode surface. Although the reactions can be reversed, the rates involved are slow, since the surface is not at equilibrium at zero-current or open-circuit on the time scale of these experiments (0.3 to several minutes).

The total charge associated with the surface processes was estimated from the current–time transient of an electrode oxidized by a potential jump from the restpotential and from the cathodic current–voltage response measured after polarizing arsenopyrite at 0.9 V for different times. Figure 6 shows two examples of such experiments in 1 M NaCl and 1 M $NaClO_4$ at pH 2 and 25 °C. In Fig. 6(a), for an electrode stepped to 0.74 V, a current-spike is clearly evident superimposed on a practically constant residual current. The charge associated with the current-spike is

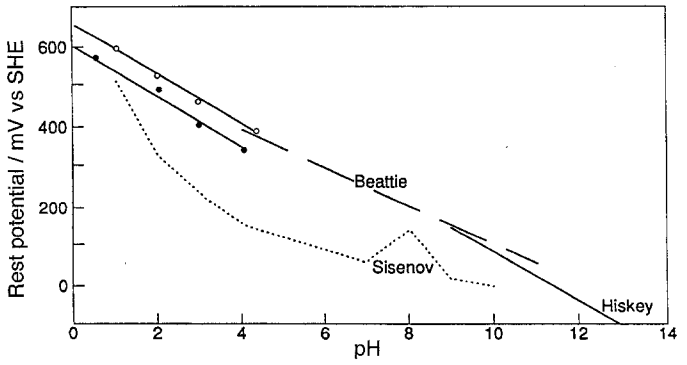

Fig. 4. Restpotential/pH dependence of arsenopyrite at 25 °C in acidified 1 M $NaClO_4$, acidified 1 M NaCl and comparison with literature values – water, Beattie [11], 0.6 M Na_2SO_4, Hiskey [15, 16] and 0.1 M KH_2PO_4, Sisenov [12]. Key: (●) rest potential in 1 M NaCl; (○) rest potential in 1 M $NaClO_4$.

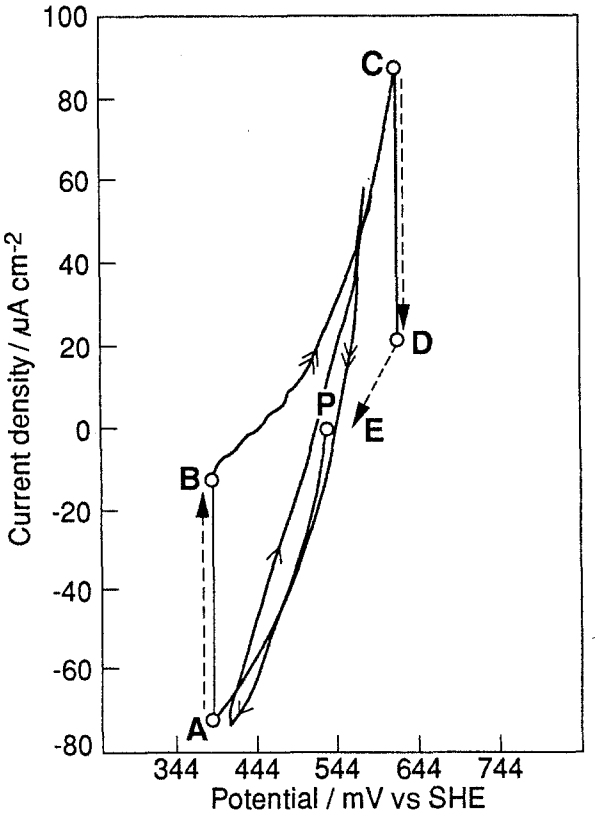

Fig. 5. Cyclic oxidation/reduction at Santa Eulalia arsenopyrite in 1 M $NaClO_4$, 10 mV s^{-1}, pH 2 at 25 °C about the restpotential P (refer to text for discussion of other symbols).

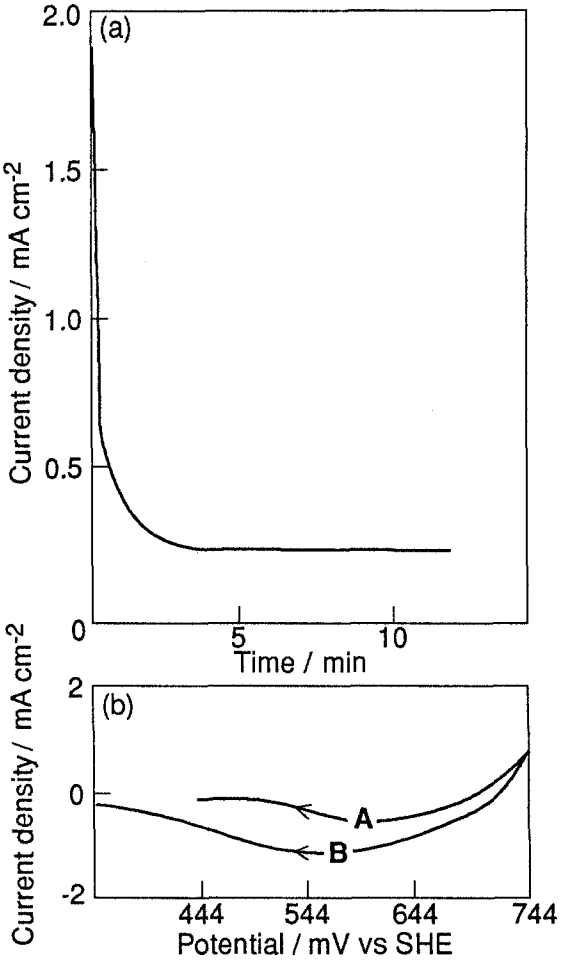

Fig. 6. Current–time behaviour of Santa Eulalia arsenopyrite at pH 2, 25 °C (a) Electrode stepped from restpotential to 0.74 V vs SHE in 1 M NaCl. (b) Electrode reduced at 10 mV s^{-1} after oxidation at 0.9 V vs SHE in 1 M $NaClO_4$ for (A) 1 and (B) 5 min, respectively.

28 mC cm^{-2} and the pattern shows that the associated reaction is completed in about 3 min. At lower potentials, the behaviour is similar but less charge is associated with the spike indicating incomplete oxidation of the surface layer. At higher potentials, the spike is less clearly resolved, because the residual current is much higher. Figure 6(b) shows reduction sweeps (A and B) after oxidizing the electrode at 0.9 V for 1 and 5 min, respectively. In each case, the cathodic reduction waves are relatively shallow, commencing about 0.2 V positive of the restpotential, with peak potentials depending on the reduction charge. For curve (A), the anodic charge passed was 1 C cm^{-2} and the cathodic charge amounted to 9 mC cm^{-2}; for curve (B), the anodic charge passed was 4.4 C cm^{-2} and the cathodic charge was 23 mC cm^{-2}. These results suggest that the oxidation/reduction capacity of the surface layer is preserved during the bulk oxidation of the mineral, with a value $\sim$ 25 mC cm^{-2} in 1 M electrolyte at pH 2 and 25 °C.

The electronic structure of arsenopyrite is uncertain [28]. The ionic approximation is $Fe^{3+}(AsS)^{3-}$ but the arsenopyrite surface converts to an oxidized metal-deficient sulfide phase when in contact with humid air or solutions [29]. In aerated acid, the composition of the surface was $FeAsS_{1.8}$ with some oxygen but no elemental sulfur present. This phase has a pyrrhotite-like structure and is stable in acidic solution and evidently in equilibrium with the underlying bulk arsenopyrite structure for hours, or longer. The initial drift of the potential of freshly prepared arsenopyrite results from the transformation of the oxidized surface produced by wet grinding in air by acid dissolution of metal ions and metal-oxide surface skeletons to form a phase such as that observed by Buckley and Walker [29]. This phase defines the restpotential of the electrode and can be semi-reversibly oxidized and reduced, thus limiting the upper oxidation state of iron $\leqslant 3$, arsenic $\leqslant 3$ and sulfur <0.

A general equilibrium governing the influence of pH and pCl on the restpotential of arsenopyrite in acid is Equation (2):

$$\{Ph(OH)_aCl_b\}_o + aH^+ + ne^- \rightleftharpoons \{Ph\}_r + aH_2O + bCl^- \quad (2)$$

where Ph denotes a particular Fe–As–S stoichiometry (e.g., $FeAsS_{1.8}$ [29]); {} denotes surface activity and the subscripts o and r, respectively, denote the oxidized, reduced form of the surface phase. Since the phase has to remain electrically neutral, $n = a + b \leqslant 6$. The restpotential is given by the Nernst equation. At 25 °C:

$$E_r = E_r^1 + 0.059bn^{-1}\ \mathrm{pCl} - 0.059an^{-1}\mathrm{pH} \quad (3)$$

where E_r^1 is a standard potential defining the multiple equilibrium between bulk arsenopyrite, surface phase

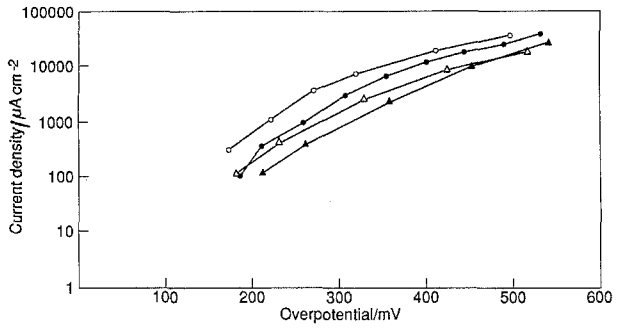

Fig. 7. Quasisteady state current–overpotential dependence of Santa Eulalia arsenopyrite in different 1 M electrolytes at pH 2 and 25 °C and effect of 0.15 M Na_2SO_4 addition. Key: (△) $NaClO_4$; (▲) NaCl; (○) $NaClO_4/SO_4^{2-}$; (●) $NaCl/SO_4^{2-}$.

and solution. In $NaClO_4$, $a = n$, $b = 0$ and the observed pH dependence of $-0.06\,V\,pH^{-1}$ is rationalized for all values of n, i.e. without needing definition of the composition of the surface phase. However, the interaction of OH^- with elements within the surface phase must be stronger than in solution since Equation 3 holds well outside the solution stability range of, for example, $Fe(OH)^{2+}$. For iron, this requirement has been confirmed by calculation [30]; the effective pK_A of $Fe(H_2O)^{3+}$ on the surface of iron oxide is −0.1 compared to the value ~ 3 in solution.

We have no systematic measurements of the dependence of E_r on pCl to fully test Equation 3. The linear pH dependence in 1 M NaCl implies that b is independent of pH. This observation suggests that the surface –Cl complex is stronger than the surface –OH complex. The most likely surface species involved is $FeCl^{2+}$, but the experimental pH dependence demands $a \sim n$, (i.e., $a > b$). If $b = 1$ and $n = 6$ the predicted slope of the pH dependence is $-0.049\,V\,pH^{-1}$, which is too low, suggesting that there may be nonequivalent iron sites in the surface phase, some of which do not bond Cl^-. Thus, for two different sites, $b = 0.5$ and the predicted slope is then $-0.054\,V\,pH^{-1}$, in increasingly better agreement with the $-0.06\,V\,pH^{-1}$ value observed experimentally.

An estimate of the thickness (Δ) of the surface phase can be obtained from the observed charge capacity, ~ 25 mC cm^{-2}. If 1 mol of the phase has a capacity of up to $6F$ (F = faraday), then $r\Delta = 25 \times 10^{-3}\,V_m/(6F)$, where r is the surface roughness and V_m the molar volume. $V_m \sim 20\,cm^3$ [28], hence $r\Delta = 8 \times 10^{-7}$ cm. If $r \sim 8$, $\Delta \sim 1$ nm which is comparable to the thickness of the surface phase estimated from XPS [29]. This calculation is suggestive rather than conclusive and assumes that the composition of the surface phase during its oxidation/reduction is constant. The presence of a metal deficient sulfide surface phase at the metal sulfide–solution interphase was initially deduced from measurements of the oxidation rate of chalcopyrite in acid [26]. The concept has since been amply verified for many metal sulfides by XPS and a good discussion of finer interpretational details is given by Walker, Richardson and Buckley [31]. The restpotentials measured in the present work represent appropriate equilibrium positions of Equation 2 for which the solution/surface phase/bulk arsenopyrite is at equilibrium. The surface phase can be oxidized/reduced concurrent with the bulk oxidation of arsenopyrite but equilibrium between the surface phase and the arsenopyrite is then uncoupled.

3.3. *Quasisteady state current – overpotential behaviour*

Figure 7 gives examples of the potential dependence of the anodic oxidation of arsenopyrite when the electrode potential is stepped from the restpotential to ~ 1 V; and the current recorded as the applied potential is reduced in steps as previously described (oxidation currents are stable for minutes, except within ~ 0.2 V of the restpotential when the reduction of the surface phase is superimposed on the oxidation reaction; currents then decrease and recover as shown by the transition A → B in Fig. 2). Potentials are expressed relative to the restpotential of the electrode. The current–overpotential dependence is initially linear (generally between 0.1–10 mA cm^{-2}) following the Tafel equation [32]: $\eta = a \log (i/i_0)$, where η = overpotential, a = Tafel slope and i_0 = exchange current density of arsenopyrite oxidation. Initially, values for $a \sim 0.12$ V, typical of an electrochemical rate controlling step involving one electron; but the current-potential dependence becomes less sensitive at higher ovepotentials, either because of a change of rate control to a nonelectrochemical step or because the effective resistance of the surface layer is potential dependent.

The effect of different variables on the reactivity of arsenopyrite was assessed from the value of i_0 obtained by extrapolating the Tafel lines to $\eta = 0$ as shown in Table 1 (estimate of uncertainty in i_0 values is ±10–20%). The data shows that Cl^- reduces the oxidation rate of arsenopyrite compared to ClO_4^-; and that in each case SO_4^{2-}, produced in the reaction [3], enhances the rate. Similarly, increased acidity and temperature enhances the rate. There is an approximate $i_0 \propto [H^+]^{0.4}$ dependence and the apparent (Arrhenius) activation energy is 33 kJ mol^{-1}.

There is no consistent rationale for the effect of anions on sulfide oxidation rates. Cation–anion (ion

Table 1. Influence of solution composition, pH and temperature on the exchange current density (i_0) for the oxidation of Santa Eulalia arsenopyrite

Electrolyte	*pH*	*Temperature*/°C	$i_0/\mu A\,cm^{-2}$
1 M NaCl	2	25	2.8
1 M NaCl/0.15 M Na_2SO_4			7.2
1 M $NaClO_4$			4.8
1 M $NaClO_4$/0.15 M Na_2SO_4			21
1 M $NaClO_4$	1	25	15
	2		4.8
	3		1.8
1 M $NaClO_4$/0.15 M Na_2SO_4	2	25	21
		50	50
		75	110

pair) interactions or complexation in solution are possible factors but undefined variables must also play a part since, for example, Jones and Peters [33] and Dutrizac [34] found that chalcopyrite oxidizes more rapidly in chloride solution than in sulfate solution while Biegler and Swift [35] reported the opposite effect. The present results agree with [8] that arsenopyrite oxidizes faster in H_2SO_4 than in HCl and the effect of pH with [18] that pressure leaching of arsenopyrite is faster in more acidic solution. The fractional dependence of i_o on $[H^+]$ has the form of an adsorption isotherm, suggesting that protons adsorbed on the surface influence the rate controlling step. The dependence of the restpotential on $[Cl^-]$ implied that Cl^- stabilized cations in the surface layer and the influence of Cl^- on the oxidation rate may have a similar origin.

3.4. *Effect of mineral stoichiometry*

Current density–potential responses of sulfur deficient (Wuhan) and arsenic deficient (Santa Eulalia) arsenopyrite were compared to stoichiometric samples (Greenbushes). The behaviour was indistinguishable. Table 2 lists the range of quasisteady state current densities at 0.9 V for each of the three samples in stirred, deaerated 0.01 M KCl at pH 2 and 25 °C.The different values overlap indicating that mineral stoichiometry does not significantly influence the oxidation rate of arsenopyrite.

This behaviour is consistent with results [35, 36] for pyrite even though the most recent and comprehensive analysis of the oxidation mechanism of pyrite involves semiconductor concepts [19, 37]. However, the lack of sensitivity of arsenopyrite reactivity to its stoichiometry could reflect an independence of the surface phase composition on bulk stoichiometry, see Equation 2.

3.5. *Long term oxidation rate*

The oxidation rate of arsenopyrite at longer times (>5 h) was obtained from the time variation of total dissolved iron (Fe) from experiments carried out for the determination of the reaction stoichiometry. This work [3] showed that for all samples one mol of Fe is derived from each mol of arsenopyrite oxidized. The value of dFe/dt is proportional to the current as the number of electrons passed per mol of arsenopyrite was constant at each temperature, ranging from 9 to 7.5 between 25 °C and 75 °C. Figure 8 shows typical graphs of Fe against time at the low (0.74 V) and high (0.94 V) end of the potential range investigated. At 0.74 V, the relationship is linear but at 0.94 V the oxidation rate increased with time. This last trend was typical of most data. Representative values for the rate at the start of oxidation and at the end of each experiment, calculated from tangent lines as illustrated in Fig. 8, are tabulated in Table 3 for 0.01 M KCl solutions at pH 2 between 25 °C and 75 °C.

Increases of the long-term oxidation rate arise from the influence of dissolved SO_4^{2-} on the oxidation rate as it is a reaction product [3]; and from enlargement of the real surface area of the electrode as the oxidation reaction proceeds. The surface area increase is apparent from microscopic examination of electrode surfaces at various stages during the reaction. Numerous small holes developed in the mineral surface which slowly receded from the plane of the surrounding epoxy resin electrode body. This space was filled progressively by a thick, flaky non-uniform white/yellow layer, which was identified as α-sulfur by XRD and SEM analysis; a colour photograph of the surface of a practically dissolved electrode is shown in [20]. We have no quantitative data for the changing electrode surface topography or for the influence of SO_4^{2-} on the rate. Therefore, the rate at the start of the reaction was used to consider different rate determining steps for the oxidation of arsenopyrite. Such analysis helps practical exploitation of the reaction to find conditions for which oxidation becomes limited by mass transport, as control by such a step implies that the chemistry of the reaction has been optimized.

Solution stirring had no influence on the oxidation rate (R) eliminating ion diffusion in the hydrodynamic Nernst layer [32] as a sole or partial controlling factor. Ion diffusion through the sulfur layer on the arsenopyrite surface could control the reaction [26]. This layer is porous because there is a decrease in the molar volume of the surface phase when arsenopyrite is converted to sulfur (molar volume change from $\sim 27\,cm^3$ to $\sim 16\,cm^3$). The thickness (L) of the sulfur layer when Fe moles of arsenopyrite has been oxidized is given [26] by $L = Fe\,V_m A^{-1}$, where V_m is the molar

Table 2. Current density (Quasisteady state measurement in stirred deaerated 0.01 M KCl at pH 2 and 25 °C) at 0.9 V vs SHE for stoichiometric (Greenbushes), arsenic deficient (Santa Eulalia) and sulfur deficient (Wuhan) arsenopyrite

Types of arsenopyrite	*Range of current density* /mA cm^{-2}
Greenbushes (Australia) $Fe_{1.00}As_{1.00}S_{1.00}$	0.71 ± 0.09
Santa Eulalia (Mexico) $Fe_{1.00}As_{0.92}S_{1.00}$	0.78 ± 0.18
Wuhan (China) $Fe_{1.00}As_{1.00}S_{0.94}$	0.83 ± 0.16

Table 3. Range of oxidation rate of Santa Eulalia arsenopyrite (μmol cm^{-2} h^{-1}) in 0.01 M KCl at pH 2 between 25 °C and 75 °C and 0.7 and 1 V vs SHE*

Potential /V vs SHE	*Temp* /°C	*Time range* /h	*Oxidation rate* /μmol cm^{-2} h^{-1}
0.74	25	125	0.9–1.3
0.84		75	4.3–9.9
0.94		30	10–16
0.84	75	5	27–45

* Rate expressed per unit geometric area of the electrode at the start of the experiment. Current equivalence is 8.7 (25 °C) and7.5 (75 °C) e^- per mol FeAsS with congruent dissolution of arsenopyrite for each condition [3].

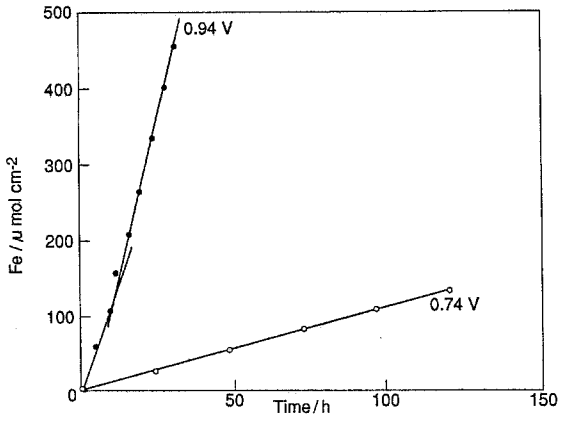

Fig. 8. Time-variation of dissolved Fe for Santa Eulalia arsenopyrite oxidation in stirred, deaerated 0.01 M KCl at pH 2, 25 °C at two potentials (the oxidation of arsenopyrite is congruent and involves ~ $9e^-$ per mol arsenopyrite oxidized [3] at each potential.

volume of arsenopyrite and A the electrode area. If the average tortuosity of a pore is τ, the effective diffusion path lengths is τL. In the early stages of the reaction at 25 °C (Fig. 8), $Fe \sim 100\,\mu\text{mol cm}^{-2}$; hence $L = 26 \times 10^{-4}$ and [26] $R = (C - C_0)D/(\tau L)$, where C is the ion surface solution concentration, C_0 is the ion bulk solution concentration and D the ion diffusion coefficient. If arsenopyrite oxidation is much faster than ion diffusion, the surface concentration of dissolved species would be limited by their solubility. The reaction produces H^+ [3], therefore the surface solution acidity must exceed that of the bulk (pH 2), preventing hydrolysis of Fe at the surface. All product species are quite soluble and, as an estimate, C is set as typically 1 M (i.e., $10^{-3}\,\text{mol cm}^{-3}$), $C_0 \sim 0$, $D \sim 10^{-5}\,\text{cm}^2\,\text{s}^{-1}$ [32]. Since R exceeds $1\,\mu\text{mol cm}^{-2}\,\text{h}^{-1}$ (Table 3), τ must exceed 10^3 for this mechanism to match the measured rate. Realistic values for τ are 1–10 [26] showing that pore-diffusion provides for much higher rates than measured. A full analysis [26] of pore-diffusion kinetics shows that the oxidation rate decreases with time ($R \propto t^{-1/2}$). This rate decrease could have been hidden in the results because of the concomitant increase in real electrode surface area and the accelerating effect of SO_4^{2-}. However, the expected activation energy for this reaction step is $\sim 10\,\text{kJ mol}^{-1}$ [26] which is much lower than the observed value of $33\,\text{kJ mol}^{-1}$. Hence pore diffusion does not control the reaction.

The high experimental activation energy, the influence of electrode potential and solution pH all suggest that the rate of oxidation of arsenopyrite is controlled by a reaction at the surface of arsenopyrite; and that increased temperature, high potential (obtained for a slurry by appropriate choice of oxidant, for example, chlorine solution) and high acidity are the primary variables to drive the reaction closer to control by mass transport of dissolved species.

4. Conclusions

Arsenopyrite can be oxidized in dilute acid under ambient conditions. The restpotential of arsenopyrite represents an equilibrium between the bulk phase, a metal deficient surface layer and the solution. The surface layer can be separately oxidized and reduced but its influence on the bulk oxidation reaction remains uncertain. Arsenopyrite oxidation appears to be controlled by an electrochemical surface reaction step with an apparent activation energy of $33\,\text{kJ mol}^{-1}$. There is no influence of mineral stoichiometry on the oxidation rate but dissolved sulfate increases the rate. Long term oxidation rates of arsenopyrite show a steadily increasing rate arising from the sulfate produced in the reaction and from an increased real surface area, clearly seen by microscopy.

Acknowledgements

Jim Graham determined the stoichiometry of arsenopyrite samples. Harold Hughes provided valuable discussion. Joanne Slattery typed the manuscript. The work was supported in part by a CSIRO–Curtin University–Industry scholarship and by the A. J. Parker Cooperative Research Centre for Hydrometallurgy.

References

[1] S. R. La Brooy, H. G. Linge and G. S. Walker, *Minerals Engineering* **7** (1994) 1213.
[2] H. G. Linge and W. G. Jones, *ibid.* **6** (1993) 873.
[3] P. G. Fernandez, H. G. Linge and M. J. Willing, *J. Appl. Electrochem.* **26** (1996) 585.
[4] H. G. Linge, 6th Aus. I. M. M. Extractive Metallurgy Conference Brisbane, July 1994, Aus.I.M.M. Melbourne (1994) p. 193.
[5] D. F. A. Koch, *in* 'Modern Aspects of Electrochemistry', vol 10 (edited by J. O'M. Bockris and B. E. Conway) Plenum, New York, (1975) p. 211.
[6] R. T. Lowson, *Chem. Rev.* **82** (1982) 461.
[7] J. Dutrizac, *Hydrometallurgy* **29** (1992) 1.
[8] G. M. Kostina and A. S. Chernyak, *J. Appl. Chem. USSR* **49** (1976) 1566.
[9] *Idem, ibid.* **50** (1977) 2571.
[10] *Idem, ibid.* **52** (1979) 1457.
[11] M. J. V. Beattie and G. W. Poling, *Ing. J. Mineral Process.* **20** (1987) 87.
[12] G. K. Sisenov, V. A. Bogdanovskaya and M. R. Tarasevich, *Soviet Electrochem.* **24** (1988) 729.
[13] J. B. Hiskey and V. Sanchez, *in* 'Arsenic Metallurgy Fundamentals and Application', TMS–AIME, Warrendale, PA (1988) p. 59.
[14] V. Sanchez and J. B. Hiskey, *Met. Trans. B* **19** (1988) 943.
[15] V. Sanchez and J. B. Hiskey, *in* 'Electrochemistry in Mineral and Metal Processing', vol. 2, Electrochemical Society, NJ, (1988) p. 264.
[16] V. Sanchez and J. B. Hiskey, *Min. & Metall. Process.* **8** (1991) 1.
[17] K. J. Jackson and J. D. H. Strickland, *Trans. Met. Soc. AIME* June (1958) 373.
[18] V. G. Papangelakis and G. P. Demopoulos, *Can. Met. Quart.* **29** (1990) 13.
[19] F. K. Crundwell, *Hydrometallurgy* **21** (1988) 155.
[20] P. G. Fernandez, PhD thesis, Curtin University of Technology, Perth (1992).
[21] N. Morimoto and L. A. Clark, *Amer. Mineralogist* **46** (1961) 1449.
[22] G. H. Aylward and T. J. V. Findlay, 'SI Chemical Data', Wiley, New York (1974).
[23] P. B. Barton, *Geochimica et Cosmochimica Acta* **33** (1969) 841.
[24] W. W. Barker and T. C. Parks, *ibid.* **50** (1986) 2185.
[25] R. von Blachnik, A. Hoppe and U. Winkel, *Z. Anorg.Allg.Chem.* **463** (1980) 78.

[26] H. G. Linge, *Hydrometallurgy* **2** (1976) 51.
[27] J. P. Arnold and R. M. Johnson, *Talanta* **16** (1969) 1991.
[28] R. T. Shuey, 'Semiconducting Ore Minerals', Elsevier Scientific, Amsterdam (1975).
[29] A. N. Buckley and G. W. Walker, *Appl. Surf. Sci.* **35** (1988/89) 227.
[30] M. A. Blesa, P. J. Morando and A. E. Regazzoni, 'Chemical Dissolution of Metal Oxides', CRC Press, Boca Raton, FA (1994).
[31] G. W. Walker, P. E. Richardson and A. N. Buckley, *Int. J. Miner. Process.* **25** (1989) 153.
[32] K. J. Vetter, 'Electrochemical Kinetics', Academic Press, New York (1967).
[33] D. L. Jones and E. Peters, *in* 'Extractive Metallurgy of Copper', TMS–AIME, New York, (1976) p. 633.
[34] J. E. Dutrizac and R. J. C. MacDonald, *Met. Trans.* **2** (1971) 2310.
[35] T. Biegler and D. A. Swift, *Electrochim. Acta* **24** (1979) 415.
[36] G. Springer, *Trans. Inst. Min. Metall.* **79** (1970) C11.
[37] K. Osseo-Asare, *Hydrometallurgy* **29** (1992) 61.